

Matching Non-Identical Objects

Yusuke Marumo^{1†} Kazuhiko Kawamoto^{2†} Satomi Tanaka^{3‡} Shigenobu Hirano^{4‡} Hiroshi Kera^{5†*}

[†]Chiba University [‡]Ricoh Company

¹yusuke.marumo@chiba-u.jp, ²kawa@faculty.chiba-u.jp, ³satomi.st.tanaka@jp.ricoh.com

⁴shigenobu.hirano@jp.ricoh.com, ⁵kera@chiba-u.jp

Abstract

Not identical but similar objects are ubiquitous in our world, ranging from four-legged animals such as dogs and cats to cars of different models and flowers of various colors. This study addresses a novel task of matching such non-identical objects at the pixel level. We propose a weighting scheme of descriptors that incorporates semantic information from object detectors into existing sparse image matching methods, extending their targets from identical objects captured from different perspectives to semantically similar objects. The experiments show successful matching between non-identical objects in various cases, including in-class design variations, class discrepancy, and domain shifts (e.g., photo–drawing and image corruptions).

1. Introduction

We humans are able to find fine-grained and robust visual correspondences between two objects even when they are not necessarily identical or when they are captured in different situations. Thanks to this ability, for example, we can find out our missing cats in a gloomy backstreet by remembering them basking in the sun or assembling components to build a shelf based on their perspective drawing. In computer vision words, this needs fine-grained matching of feature points between two objects even with class discrepancy and domain shift (e.g., image corruptions).

The abovementioned matching has been partially addressed in the literature. In the image matching [17, 27, 49, 56], objects to be matched are assumed identical and captured from different perspectives. This assumption also enables supervised training using dense correspondence obtained from 3D reconstruction from image pairs. Recently, Transformer-based dense matching methods have shown great performance [5, 11, 23, 45, 56, 67, 72, 74], and there are also light-weight sparse matching methods, which run in real time with a slight cost in accuracy [17, 22, 30, 38,

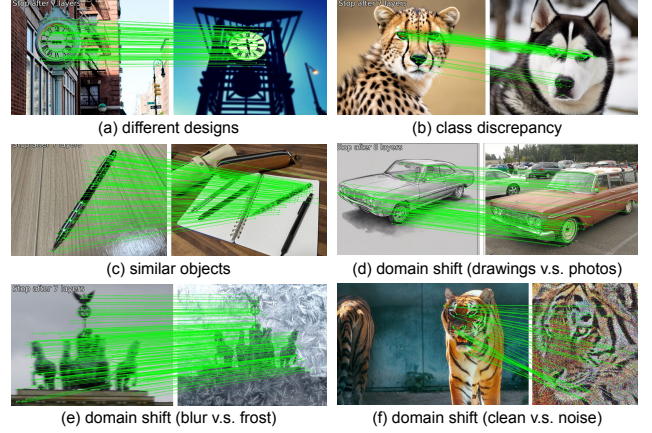


Figure 1. Non-identical object matching by our plug-and-play module incorporated with the sparse image matching pipeline (here, SuperPoint [10] for keypoint detection and LightGlue [27] for matching). (a) design differences, (b) class discrepancy, (c) similar objects, and domain shifts such as (d) drawing v.s. photo and (e, f) different image corruptions.

46, 49, 66]. In contrast, semantic correspondence models [7, 32, 70] focus on matching semantically similar parts between objects (e.g., tires of two bikes). They are trained on datasets with sparse part-to-part correspondence annotation and thus do not offer fine-grained matching.

In this study, we generalize image matching and semantic correspondence to *non-identical object matching*, where objects to be matched are not necessarily identical (see Fig. 1). For example, the object pair can be street clocks of different designs or four-legged animals of different species. Further, the non-identity naturally requires robustness, e.g., against image corruptions (e.g., blurs and brightness change) and domain shifts (e.g., photo v.s. drawing) because two objects may be captured in different environments and domains. A crucial challenge of achieving non-identical object matching is that we cannot straightforwardly resort to the supervised learning framework because of the ambiguity of non-identity; there is no ground-

*Corresponding Author.

truth matching between non-identical objects.

We propose a simple plug-and-play weighting module that extends off-the-shelf sparse matching methods to non-identical object matching. Given a pair of images, existing sparse matching methods first perform keypoint detection and then feed the extracted descriptors to a feature matching model to determine the matching of the keypoints. Our weighting module is inserted before the feature matching model and weights the descriptors using semantic information. Particularly, we introduce an object detector to identify objects and compute a Grad-CAM heatmap [51] to obtain weights. Previously, because of the task definition, matching methods only exploit low-level features, such as colors, edges, and texture, which are all susceptible to ambiguities and perturbations appearing in the non-identical object matching task (see Fig. 2). The low-level features are still essential to realize fine-grained matching, but the proposed module makes it robust using high-level features. Further, to avoid emphasizing irrelevant objects when an image contains more than one object, we propose *Class Similarity Adapter*, which determines the most relevant object pairs. We leverage the class labels from an object detector and determine object pairs based on their semantic similarity in the text embedding space.

Our experiments demonstrate that our approach significantly boosts the robustness of sparse matching methods, including LightGlue [27] and GlueStick [38], in two tasks: non-identical object matching and robust image matching. In the former task, we evaluate the matching results with various image pairs (a) of the same class, (b) with class discrepancy, (c) with domain shift, and (d) of the same appearance. The sparse matchers alone result in scattered mismatching between non-corresponding areas, but combined with our method, fine-grained and consistent matching is achieved. In the latter task, we evaluate the robustness of matching on the MegaDepth-1500 [56] dataset under common corruptions [20] in terms of the AUC score of standard relative pose estimation. Our method outperforms the state-of-the-art sparse matcher under various types of image corruptions. The average AUC of our method even exceeds that of dense matchers, LoFTR [56] and Efficient LoFTR [64], which pursue matching quality at the cost of speed.

To summarize, our contributions are as follows:

- We tackle non-identical object matching, a novel task of matching similar but unnecessarily identical objects in images, even under image corruptions and/or between different domains, which can be considered a generation of classical image matching and semantic correspondence.
- We propose a simple plug-and-play weighting module that enhances the low-level features using semantic information and successfully extends various sparse matching methods to non-identical object matching.
- We present a first evaluation of the robustness in image

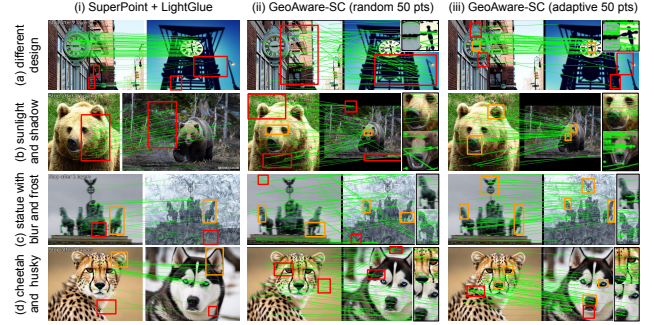


Figure 2. Failure cases of non-identical object matching using the state-of-the-art matcher, LightGlue [27], and the semantic correspondence model, GeoAware-SC [70]. In semantic correspondence models, some points indicating object parts must be designated during inference to find correspondences, and automating this point selection is essential for feature point matching. Comparison of feature matching by GeoAware-SC using two methods: one that randomly extracts 50 points and the other that adaptively extracts 50 points based on the GradCAM [51] heatmap of YOLOv7 [62]. Red boxes indicate mismatches due to background or object-like textures. Orange boxes indicate semantically corresponding regions, where most points align at a part level but not at a pixel level. For example, in (d), mismatches occur between the tip of the nose of the cheetah and the nostrils of the husky.

matching under common corruptions. By adding corruptions to both input images, the robustness against corruptions itself is measured. By adding them to only one of the input images, the robustness against a domain shift is measured. For both cases, our method is shown useful.

2. Related Work

Image matching [17, 27, 49, 56] is a fundamental task in computer vision with various applications [8, 34, 35, 43, 50, 55, 57, 63] that involves finding the fine-grained correspondence between two images. Many image matching methods have two stages. A keypoint detector first extracts keypoints with their positions and local feature descriptors, and then feature matchers find correspondences between them.

Keypoint detectors. Classically, keypoint detection was done using hand-crafted local features such as SIFT [28] and ORB [48]. Recently, learning-based methods have been developed [10, 12, 14, 18, 41, 61]. Particularly, SuperPoint [10] and DISK [59] are two popular examples. The former is based on convolutional neural networks, and the latter is based on reinforcement learning. There is also a fully differentiable and lightweight method with a minimal model configuration [14]. Unsupervised keypoint detection based on a text-to-image diffusion model [18] also exists.

Feature matchers. Feature matchers [65, 68] find a fine-grained correspondence between images. The feature matchers are categorized into two types based on the density of matching points: sparse matchers and dense matchers. The former runs faster, while the latter gives dense and high accuracy. The focus of our study lies in sparse matchers. A seminal sparse matcher, SuperGlue [49], addresses the partial assignment problem for matching by integrating the Transformer attention mechanism [60] with optimal transport [40]. The state-of-the-art sparse matcher, LightGlue [27], improves SuperGlue by introducing a hierarchical matching structure, achieving high matching accuracy and real-time processing simultaneously. GlueStick [38] utilizes line segments for structural features. In contrast to sparse matchers, dense matchers [5, 11, 23, 45, 56, 67, 72, 74] peruse matching accuracy rather than speed. Dense matchers input an image and infer matching using all pixels as keypoints. Therefore, it does not require a keypoint detector, so it is also called a detector-free model. LoFTR [56] proposed the first transformer-based method for dense matching, which achieves highly dense matching. Recent studies [29, 36, 71] such as Efficient LoFTR [64], enabling fast and accurate matching by token aggregation, ASpanFormer [5], which controls the attention span, and ASTR [67], which focuses on the role of each pixel.

Semantic correspondence models. Semantic Correspondence [2, 6, 15, 16, 33] is a task of identifying a semantically similar point in the target image from the given point in the source image. Specifically, it enables the correspondence of parts, such as the mouth, nose, or right eye of dogs between the source and target images. The training of a model is conducted using a specialized dataset, such as SPair-71k [33] and PF-PASCAL [15], which employ sparsely annotated part-level correspondences as supervisory data. Recently, GeoAware-SC [70] has been proposed as a model that leverages pre-trained features from two foundational models, Stable Diffusion [47] and DINOv2 [37], integrating both geometric and semantic information. This model significantly improves accuracy on major benchmarks for semantic correspondence, including the SPair-71k [33] and PF-PASCAL [15] datasets. In recent years, various models [21, 39, 52, 58, 69] have been studied. For example, CATs++ [7], which combines the local feature aggregation capacity of CNNs with the broad contextual comprehension of transformers; a model [32] employing feature maps from the reverse diffusion process in diffusion models; and unsupervised models [19] that learn semantic correspondence without requiring annotated data.

While feature matching and semantic correspondence are also the tasks of finding correspondences, our task (i.e., fine-grained matching between non-identical objects)

is more challenging. First, it is hard to be addressed by the supervised learning framework because (i) manual annotation, as in semantic correspondence datasets is laborious for the pixel-level correspondence, and (ii) automatic annotation by 3D reconstruction, as in feature matching, which assumes an identical object viewed from different perspectives, cannot be done. Second, because non-identical objects generally appear with different lighting, image corruptions, or even image domains, the matching method should be designed to be robust to such diversity. As shown in Fig. 2, state-of-the-art feature matching methods and semantic correspondence models are susceptible to such variations. Several studies addressed robust matching with specific conditions, such as DarkFeat [17] for low-light and SAM [30] for viewpoint and illumination changes. We consider broader changes, including fifteen types of common corruptions [20] and several image domains (e.g., photos and sketches).

3. Non-Identical Object Matching

We introduce non-identical object matching, matching between unnecessarily identical objects in two images. For example, a dog and a cat are not identical but still have similar structures, such as two eyes, four legs, and one tail. The same mass-produced products, such as cars of the same model, have the same appearance but are still not identical (e.g., owned by different people) and can appear in images with largely different backgrounds and lighting conditions.

3.1. Task formulation

In the following, we present a more formal problem setup based on a standard matching pipeline. Note that it is essentially hard to completely formalize the non-identical object matching because of the ambiguity of non-identity, so our formalization is slightly conceptual.

Problem 1 (Non-identical object matching) *Let \mathcal{X} be the image domain. Given two images $\mathbf{x}_A, \mathbf{x}_B \in \mathcal{X}$, let $D_A = \{(\mathbf{p}_i^A, \mathbf{d}_i^A)\}_{i=1}^{n_A}$ be n_A keypoints in image \mathbf{x}_A , where $\mathbf{p}_i^A \in \mathbb{R}^2$ and $\mathbf{d}_i^A \in [0, 1]^d$ are the position and the descriptor of i -th keypoint, respectively. We define $D_B = \{(\mathbf{p}_i^B, \mathbf{d}_i^B)\}_{i=1}^{n_B}$ for image \mathbf{x}_B similarly. Let $\mathcal{L}(\cdot)$ be a (conceptual) matching loss function. The non-identical object matching can be formalized as follows.*

$$\min \quad \mathcal{L}(\{m_{kl}\}_{k=1, \dots, n_A, l=1, \dots, n_B}) \quad (1)$$

$$\text{s.t.} \quad m_{kl} \in [0, 1], \forall k \in \{1, \dots, n_A\}, l \in \{1, \dots, n_B\} \quad (2)$$

$$\sum_{l=1}^{n_B} m_{kl} \leq 1, \forall k \in \{1, \dots, n_A\} \quad (3)$$

$$\sum_{k=1}^{n_A} m_{kl} \leq 1, \forall l \in \{1, \dots, n_B\}. \quad (4)$$

The matching coefficient $m_{kl} = 1$ indicates that the k -th keypoint in image \mathbf{x}_A and the l -th keypoint in image \mathbf{x}_B is matched and otherwise $m_{kl} = 0$. Each keypoint in one image has at most one matched point in the other image. This condition is implemented by the last two constraints. In the image matching task, where an identical object is captured from different angles in two images, the matching loss $\mathcal{L}(\{m_{kl}\}_{k,l})$ measures the discrepancy between a camera pose computed the matching $\{m_{kl}\}_{k,l}$ and the ground truth.

Our task, non-identical object matching, covers a broader class of matching. Given two images $\mathbf{x}_A, \mathbf{x}_B \in \mathcal{X}$ that contain (potentially non-identical) objects to be matched, image \mathbf{x}_I can be characterized by several attributes (o_I, y_I, P_I, D_I) for $I \in \{A, B\}$. If $o_A = o_B$, then the objects to be matched are identical. If $o_A \equiv o_B$, they are the same in appearance but not necessarily identical (e.g., two cars of the same model). If $y_A = y_B$, they belong to the same class (e.g., the car class). If $P_A = P_B$, then they are captured from the same camera pose. If $D_A = D_B$, they are captured in the same domain (e.g., the drawing domain).

The classical image matching corresponds to the case with $o_A = o_B$ (consequently, $o_A \equiv o_B$ and $y_A = y_B$), $P_A \neq P_B$, and $D_A = D_B$. In words, it considers identical objects captured from different camera poses in the same domain. In contrast, non-identical object matching encompasses $y_A \neq y_B$ (consequently, $o_A \neq o_B$ and $o_A \not\equiv o_B$), $P_A \neq P_B$, and $D_A \neq D_B$. Note that we practically assume o_A and o_B to be *similar* in some sense. Below, we highlight two important special cases, both assuming $P_A \neq P_B$.

Class discrepancy ($y_A \neq y_B$). Four-legged animals, such as tigers and cats, are objects of different classes but have similar structures. They both have two eyes, four legs, and one tail. We humans can find a part-by-part matching between them, even with differences in color, texture, and shape. However, it is not trivial to design matching methods to find fine-grained correspondence while being robust to detail differences. If such a matching is realized, for example, one may track the running motions of unknown four-legged animals based on those of known ones.

Domain shift ($o_A \equiv o_B, D_A \neq D_B$). We humans can know the flower in the painting on the wall depicts that in the garden. This is a robust fine-grained matching of an identical object in different domains. Typical domain shifts include drawings v.s. photos and clean images v.s. corrupted images. For example, suppose that \mathbf{x}_A is a photo and \mathbf{x}_B is a painting. Compared to photos, drawings have fewer colors, textures, and shadows. Thus, while the descriptors of the photo \mathbf{x}_A may reflect the color or texture, those of the drawing \mathbf{x}_B do not, which can lead to an absent of correspondence if the feature matcher is not sufficiently robust. If robust matching between different domains is realized,

for example, one can design a system that guides a worker to assemble parts from the first-person video by comparing the parts with those in a blueprint.

3.2. Technical challenges

Generalization from image matching to non-identical object matching introduces ambiguities and perturbations into matching. First, because there is no “correct matching” between two non-identical objects (e.g., a dog and a cat), one cannot resort to a simple supervised learning framework. There is no clear measure of a good matching that can be used for computing a loss to minimize. Second, domain shifts by common corruptions or image styles significantly change the low-level features. To our knowledge, existing matching methods only use low-level features such as colors, edges, and textures. As a consequence, these methods are susceptible to the domain shift, as shown in Fig. 2. The first challenge suggests that it would be better to somehow robustify pretrained image matching models instead of training a model from scratch. The second challenge indicates the necessity of introducing semantic information, which is known to be more robust against domain shifts.

4. Proposed Method

In this section, we present a simple plug-and-play weighting module that can turn various sparse matchers to work for non-identical object matching. Most sparse matchers, such as [4, 27, 38, 49], consist of a pair of a keypoint detector and a feature matcher, and our module process the keypoints before feeding them to the feature matcher. Particularly, given a pair of images $\mathbf{x}_A, \mathbf{x}_B \in \mathcal{X}$, The keypoint detector outputs collections of keypoints $D_A = \{(\mathbf{p}_i^A, \mathbf{d}_i^A)\}_i, D_B = \{(\mathbf{p}_i^B, \mathbf{d}_i^B)\}_i$. The proposed module then computes weighted descriptors $\tilde{\mathbf{d}}_i^A, \tilde{\mathbf{d}}_i^B$ for each $\mathbf{d}_i^A, \mathbf{d}_i^B$, respectively. Lastly, the feature matcher performs matching using $\tilde{D}_A = \{(\mathbf{p}_i^A, \tilde{\mathbf{d}}_i^A)\}_i, \tilde{D}_B = \{(\mathbf{p}_i^B, \tilde{\mathbf{d}}_i^B)\}_i$.

4.1. Weighting module

The proposed weighting module uses an object detector and visual explanation model. This study used YOLOv7 [62] and Grad-CAM [51]. Let $\mathbf{x} \in \mathcal{X}$ be an image, and let $D = \{(\mathbf{p}_i, \mathbf{d}_i)\}_{i=1}^n$ be the collection of n keypoints of \mathbf{x} .

First, the object detector is applied to \mathbf{x} and detects the objects with their classes. For each of the detected objects (say, the k -th object), the visual explanation model gives pixel-wise class-activation scores or a heatmap H_k . Let $H_{k, \mathbf{p}_i} \in [0, 1]$ be the heatmap score of H_k at \mathbf{p}_i . Then, the heatmap scores at \mathbf{p}_i are aggregated as $H_{\mathbf{p}_i} := \max_k H_{k, \mathbf{p}_i}$. Finally, the weighted descriptor $\tilde{\mathbf{d}}_i$ is computed by

$$\tilde{\mathbf{d}}_i = \frac{1 + H_{\mathbf{p}_i}}{\max_{j \in \{1, \dots, n\}} (1 + H_{\mathbf{p}_j})} \cdot \mathbf{d}_i \in [0.5, 1]^d. \quad (5)$$

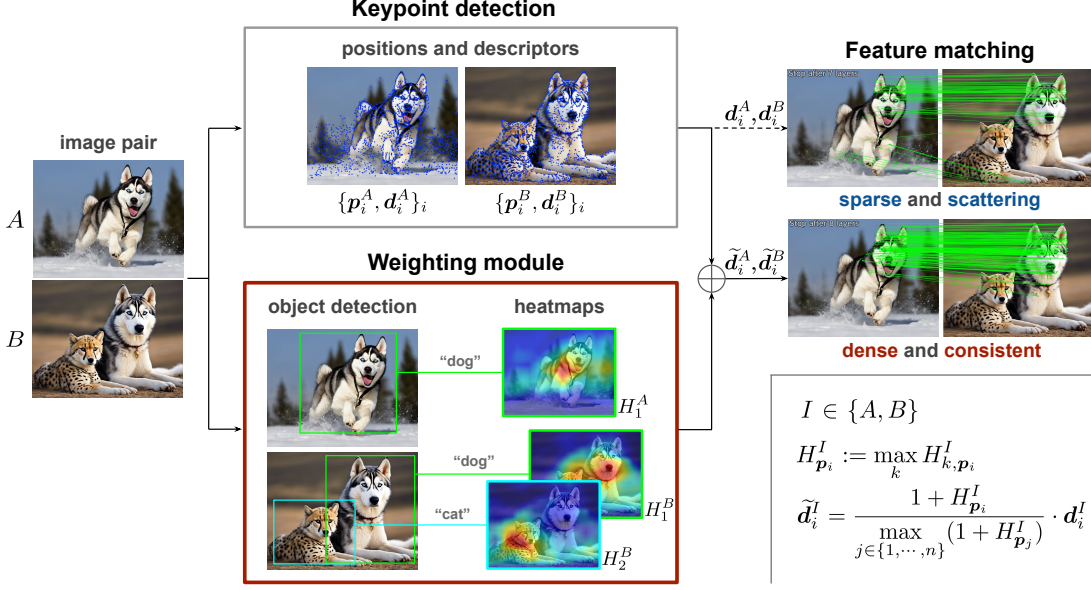


Figure 3. Pipeline of the matching. The keypoint detection and feature matching are done by off-the-shelf models. The proposed weighting module computes the heatmap scores of objects and weights the descriptors with this semantic information.

We empirically found that the addition of base value 1 and the normalization by the maximum is important. For example, the simplest approach $\tilde{d}_i = H_{p_i} d_i \in [0, 1]^d$ ends up with a scarcity of matching because of the heatmap scores on the keypoints on background tend to be too low, i.e., $H_{p_i} \approx 0$. Although such keypoints will not likely appear in the matching results, they seem to help the keypoints on objects to be matched. If one instead uses $\tilde{d}_i = (1 + H_{p_i}) d_i \in [1, 2]^d$, this also affects negatively. We consider that this is because of the softmax operations used in the subsequent feature matching. We discuss the consequence of the weighting of descriptors next.

4.2. Effect of weights in feature matcher

We now illustrate how our weighting module affects the subsequent feature matching. We take LightGlue [27] as an example, but a similar discussion holds for other feature matchers. For simplicity, let α_i be the weight in Eq. (5), i.e., $\tilde{d}_i = \alpha_i d_i$. The matcher takes as input the keypoints $\tilde{D}_A = \{(p_i^A, \tilde{d}_i^A)\}_i$, $\tilde{D}_B = \{(p_i^B, \tilde{d}_i^B)\}_i$. The vectors $\tilde{d}_i^A = \alpha_i^A d_i^A$, $\tilde{d}_i^B = \alpha_i^B d_i^B$ are the i -th weighted descriptors of image x_A, x_B , respectively. Below, symbols with and without $\tilde{\cdot}$ present those with and without weighting.

In the feature matcher, the descriptors are first converted to key and query vectors using matrices $W_q, W_k \in \mathbb{R}^{d \times d}$.

$$\tilde{q}_i^I = W_q \tilde{d}_i^I = \alpha_i W_q d_i^I = \alpha_i q_i^I \quad (6)$$

$$\tilde{k}_i^I = W_k \tilde{d}_i^I = \alpha_i W_k d_i^I = \alpha_i k_i^I, \quad (7)$$

where $I \in \{A, B\}$. Then, the self-attention score a_{ij}^I be-

tween i -th and j -th keypoints of image x_I is calculated as¹

$$\tilde{a}_{ij}^I = \tilde{q}_i^{I\top} \mathcal{R}(p_j^I - p_i^I) \tilde{k}_j^I \quad (8)$$

$$= (\alpha_i^I \alpha_j^I) \cdot (q_i^{I\top} \mathcal{R}(p_j^I - p_i^I) k_j^I) \quad (9)$$

$$= (\alpha_i^I \alpha_j^I) \cdot a_{ij}^I, \quad (10)$$

where $\mathcal{R} : \mathbb{R}^2 \rightarrow \mathbb{R}^{d \times d}$ denotes the rotary-encoding [53]. Therefore, our weighting by heatmap scores leads to the weighting of attention scores. The self-attention scores reflect the internal relationship of objects and background, thereby extracting better feature representations in the subsequent steps of the feature matcher. Roughly speaking, nothing that $\alpha_i^I \in [0.5, 1.0]$ for all i and $I \in \{A, B\}$, we have $\alpha_i^I \alpha_j^I \approx 1$ between the keypoints on objects, $\alpha_i^I \alpha_j^I \approx 0.5$ between one on object and the other on background, and $\alpha_i^I \alpha_j^I \approx 0$ for between those on the background. This is reasonable because we want nice feature representations for object keypoints for nice matching. Nevertheless, such nice representations should be obtained by taking into account the background conditions, e.g., to compensate for the overall lighting conditions. If one uses $\alpha_i^I = H_{p_i}$ as discussed earlier, i.e., $H_{p_i} \approx 0$ for background keypoints, the feature representations cannot take into account the background.

Similarly, our weighting affects the cross-attention score a_{ij}^{AB} between the i -th keypoint of image x_A and the j -th keypoint of image x_B , computed from the key vectors.

$$\tilde{a}_{ij}^{AB} = \tilde{k}_i^{A\top} \tilde{k}_j^B = (\alpha_i^A \alpha_j^B) \cdot a_{ij}^{AB}. \quad (11)$$

¹To be precise, this score should be considered as the pre-activation score, and the softmax operation will be subsequently applied. The terminology of this paper follows the related studies, e.g., [27].

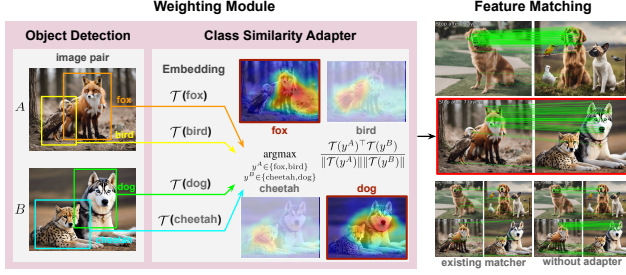


Figure 4. Class Similarity Adapter converts class labels from an object detector into embeddings using the CLIP [42] text encoder and compares them with cosine similarity to identify semantically similar object pairs. The GradCAM [51] heatmap of object detector YOLOv7 [62] generated for the chosen object pair is used for our weighting method, enhancing matching with multiple objects. Here, we used the keypoint detector SuperPoint [10] and the feature matcher LightGlue [27].

As discussed earlier, the value of $\alpha_i^A \alpha_j^B$ is generally large between the keypoints on objects. Clearly, this encourages the matching between objects.

4.3. Class Similarity Adapter

We propose the *Class Similarity Adapter* to address scenarios where multiple objects are present in an image. Our weighting module uses all heatmaps of objects detected by the object detector for weighting. However, this can needlessly emphasize irrelevant objects, leading to scattered matching from one to multiple objects. As shown in Fig. 4 (bottom right), relying solely on visual information leads to matching based on similarities in texture, color, and shape, where similar black features such as the nose of the dog and the ear of the cat, are incorrectly matched, causing correspondences to scatter across multiple animals.

To resolve such confusion in the visual space, we again leverage semantic information given by the object detector. Particularly, we map the class labels of detected objects to text embedding space and determine the object pair to be matched based on the cosine similarity between embedding vectors. Suppose that an image x_A contains n_A objects, and let $Y_A = \{y_i^A\}_{i=1}^{n_A}$ be their class labels. We define $Y_B = \{y_i^B\}_{i=1}^{n_B}$ similarly for the other image x_B . Let \mathcal{T} be a pretrained text encoder that maps a label y to an embedding vector $\mathcal{T}(y)$. Particularly, we used the CLIP text encoder [42]. The Class Similarity Adapter determines the object pair (i, j) to be matched based on the cosine similarity between the embedding vectors as follows.

$$(y_i^A, y_j^B) = \underset{y^A \in Y_A, y^B \in Y_B}{\operatorname{argmax}} \frac{\mathcal{T}(y^A)^\top \mathcal{T}(y^B)}{\|\mathcal{T}(y^A)\| \|\mathcal{T}(y^B)\|}, \quad (12)$$

where $\|\cdot\|$ denotes the L_2 norm of vector. Then, the weighting module only uses the Grad-CAM heatmaps of the i -th

object in x_A and the j -th object in x_B . Based on this result, the weighting module uses the corresponding heatmaps for weighting the descriptors. Figure 4 shows this pipeline.

5. Experiments

We demonstrate the effectiveness of our method in non-identical object matching tasks, presenting qualitative results on various pairs of non-identical (but similar) objects, followed by quantitative evaluation on classical image matching tasks but under common corruptions [20].

Setup. In the sparse matching framework, the image matching task is performed by a keypoint detector and a feature matcher. For the former, we adopted pre-trained SuperPoint [10], extracting 2,048 keypoints. For the latter, the extracted keypoints are matched using either pre-trained SGMNet [4], GlueStick [38], and the state-of-the-art method, LightGlue [27], with and without the proposed weighting module. We additionally tested a detector-free dense matcher, LoFTR [56] and Efficient LoFTR [64]. We downloaded the pretrained models from their official repositories (details provided in the supplementary material). All experiments are conducted on a computer with an NVIDIA GeForce RTX 3090 GPU and 24GB memory.

5.1. Matching Non-Identical Objects

In this experiment, we address a matching of non-identical objects. It is worth noting that this task can only be qualitatively evaluated because there is no ground truth matching between non-identical objects.

Datasets. We collected various images with objects from the COCO [26] and ImageNet [9] datasets. To prepare the drawing version of several images, we used the DreamStudio², which is backed by the Stable Diffusion [47].

Robust matching across non-identical objects. We examined four cases: (i) same class (i.e., $y_A = y_B, D_A = D_B$), (ii) class discrepancy (i.e., $y_A \neq y_B, D_A = D_B$), (iii) domain shift (i.e., $o_A \equiv o_B, D_A \neq D_B$), and (iv) same appearance (i.e., $o_A = o_B$). For all the cases, we have perspective difference (i.e., $P_A \neq P_B$). Due to the page number restriction, we only present a limited number of matching examples here, but more results can be found in Sec. A in the supplementary material. Figure 5 shows the matching results with and without the proposed method in the four cases. As can be seen in Fig. 5(a), a combination of SuperPoint and LightGlue cannot distinguish between objects and backgrounds or correspond to the same structure of animals. In contrast, Fig. 5(b) shows that the

²<https://beta.dreamstudio.ai/generate>

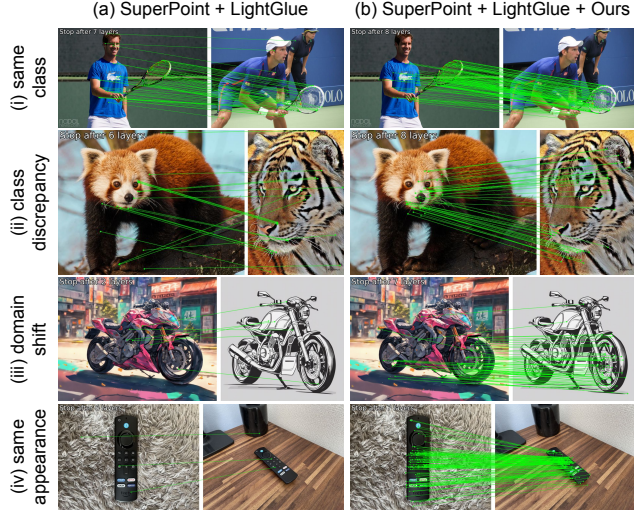


Figure 5. Typical categories of non-identical object matching. (a) A combination of SuperPoint [10] and LightGlue [27] only finds a small number of correspondence, and many of them are incorrect. (b) The proposed method significantly improves the matching.

introduction of the proposed method significantly improves the results, reducing unreasonable matchings (e.g., human and racket, animal eye and mouth) and increasing reasonable part-to-part matchings. Particularly, for the cases (i) increased the number of matches between rackets and decreased the mismatches between people, (ii) corresponded to the same parts of animals, (iii) matched front wheels with domain gaps, and (iv) significantly increased the number of matches despite changes in background and object angles. Notably, structural features, such as eyes and noses, are successfully matched between different classes. We consider that the heatmaps of these animals gave similar importance to the eyes or mouth, thus increasing the number of matches between the same parts of the body. In addition, the results for the same class and appearance showed a decrease in mismatches with the background, which means that the background and foreground had relatively lower similarity.

Different matchers. Figure 6 presents the results with other matchers, showing that our method boosts all of them to match corresponding parts between different animals.

5.2. Robust Image Matching

We next quantitatively evaluate the proposed method on a standard image matching task but with common corruptions. To our knowledge, we present the first evaluation of the robustness of image matching under common corruptions. We address two cases: (i) both input images are corrupted, and (ii) only one of them is corrupted. The former shows the robustness against corruption, and the latter shows the robustness against domain shift (i.e., clean image



Figure 6. The results with different matchers [4, 27, 38]. SuperPoint [10] is used for the keypoint detection. The introduction of our module increases the matching of eyes and noses between the cheetah and husky and decreases mismatching in the background.

domain v.s. corrupted image domain).

Dataset. We use image pairs from the MegaDepth-1500 [56] test set as the basis for various experiments. MegaDepth [25] dataset consists of 3D reconstructed data from one million images for two popular phototourism destinations, with camera poses and depth maps computed via COLMAP [50] and refined as ground truth. Common Corruptions [20] simulates the 15 types of corruptions that occur when images are captured. The severity level of corruption is set to 5, which is the most challenging condition.

Metric. We follow the standard evaluation of image matching based on relative pose estimation (e.g., see [27]). From the matching results, the relative pose between two images is computed with RANSAC [13] as follows. First, an essential matrix representing the positional transformation between the images is calculated, which is then decomposed into a rotation and a translation. The camera pose error is computed by the maximum angular error, and the area under the cumulative error curve (AUC) at 20° is calculated.

Robustness against common corruptions. The left side of Tab. 1 shows the AUC of matching when input images are both corrupted. The results of the dense matching method (i.e., LoFTR and Efficient LoFTR) are given for reference. As the results show, the proposed method makes the LightGlue and GlueStick robust against most types of common corruptions (roughly 5% to 10% increase) with a slight increase in the runtime. The average AUC even exceeds that of Efficient LoFTR. The matching methods benefit from the proposed method, particularly when images are corrupted by noises and blurs. We observe AUC decrease in a few types of corruptions, such as Snow and Frost, by the introduction of the proposed method. These corruptions introduce edgy geometric patterns, and the matching methods find correspondence between them. See Sec. B.1 in the supplementary material for more detailed comparisons.

Robustness against environmental changes. As the objects to be matched are non-identical, they can appear in

Table 1. The pose accuracy (AUC) at the maximum angular error of 20° of the relative pose estimation from image pairs MegaDepth-1500 [56] under common corruptions [20]. The left side shows both images corrupted with the same type of corruption, while the right side shows only one of the input images corrupted and the other as a clean image. Our method largely improves LightGlue (LG) [27] and GlueStick (GS) [38] for most categories and the average AUC. The dense matchers, LoFTR [56] and Efficient LoFTR (ELoFTR) [64], are shown for reference. Our method improves the robustness of sparse matchers with a slight reduction in clean accuracy and runtime.

Common Corruptions	AUC@20° with pairs of corrupted images						AUC@20° with pairs of clean and corrupted images					
	<i>keypoint detector : SuperPoint</i>			<i>dense matcher</i>			<i>keypoint detector : SuperPoint</i>			<i>dense matcher</i>		
	LG	LG+Ours	GS	GS+Ours	LoFTR	ELoFTR	LG	LG+Ours	GS	GS+Ours	LoFTR	ELoFTR
None (Clean)	80.61	78.42	78.04	75.08	80.93	83.48	80.61	78.42	78.04	75.08	80.93	83.48
Gaussian Noise	43.09	53.27	45.67	52.24	34.97	35.71	27.54	41.01	41.93	44.98	33.02	36.56
Shot Noise	43.41	53.82	46.10	51.72	40.00	40.36	32.10	42.35	41.75	43.82	36.53	39.52
Impulse Noise	44.98	50.11	44.91	50.05	37.73	39.89	35.95	43.67	40.97	42.91	34.92	38.63
Defocus Blur	32.69	48.35	45.58	49.23	57.22	54.97	18.25	32.13	23.16	30.10	49.40	41.97
Frosted Glass Blur	33.37	47.88	47.40	49.94	54.48	47.09	34.25	44.80	42.96	46.21	54.53	47.52
Motion Blur	42.12	53.63	44.76	51.84	55.60	48.12	50.07	53.10	44.27	52.69	52.81	45.10
Zoom Blur	24.40	31.21	22.87	30.97	23.08	22.54	34.67	40.04	31.18	37.11	31.09	28.49
Snow	31.51	30.33	25.26	23.21	31.85	37.89	56.24	58.15	47.22	48.53	49.15	54.56
Frost	32.24	31.71	26.39	24.22	19.23	25.49	62.20	64.87	54.34	57.26	43.17	45.18
Fog	70.99	73.49	71.19	73.89	67.10	67.74	76.96	78.40	75.18	74.87	74.06	75.36
Brightness	75.48	75.08	73.03	70.84	75.45	79.83	77.14	76.98	76.78	75.06	78.41	81.26
Contrast	39.50	38.47	39.47	42.61	53.22	59.78	43.09	45.17	40.44	43.53	39.66	52.76
Elastic Transform	54.78	66.21	60.37	64.36	58.56	60.50	64.93	68.34	68.02	69.92	68.95	71.49
Pixelate	67.94	68.24	65.01	64.81	74.77	77.27	66.80	68.43	67.16	65.46	76.21	78.45
JPEG Compression	29.54	36.97	39.66	44.70	59.05	59.80	47.41	53.82	60.39	60.12	68.14	71.70
Average	44.40	50.58	46.51	49.64	49.49	50.47	48.51	54.08	50.38	52.84	52.67	53.90
Time [ms/pair]	46.67	68.43	105.72	128.18	312.54	191.17	45.98	68.37	105.34	127.86	305.01	192.53

largely different environments. The right side of Tab. 1 shows the AUC when only one of the input images is corrupted and the other is clean. As in the left side of Tab. 1, the proposed method boosts the LightGlue and GlueStick for most cases and the average case. Interestingly, the results are better for almost all weather categories. For brightness, it is the only one of all categories that shows a decrease in accuracy, but the drop is slight. Weather categories such as Snow and Frost add strong geometry to the overall image, causing mismatches as occlusions. Heatmap weighting is considered to structurally complement the areas hidden by occlusion. The proposed method makes existing matchers robust to environmental changes in general, with a slight precision reduction in clean images. See Section B.2 in the supplementary material for more detailed comparisons.

5.3. Limitations

We here present failure cases. Figure 7 shows typical cases caused by (a) heatmaps not covering a whole part of objects and (b) great structural differences. In the former case, the importance scores take large only on particular parts of the objects. Further, the large importance scores on the irrelevant object disrupt the matching. This may be resolved by using a better visual explanation model [1, 3, 31, 54, 73]. For the latter case, objects with great structural differences cannot be matched as there is little correspondence between the objects, and eventually, regions of similar colors or tex-



Figure 7. Failure cases. (a) High heatmap scores are given to only a small region of objects to be matched. (b) The structures of objects are clearly different.

tures are matched. To address these cases, one may introduce the vision and language model, such as the segment anything model [24, 44] to complement the visual information with text and part-level mask information.

6. Conclusion

In this study, we addressed a novel task of non-identical object matching, where objects to be matched are only assumed semantically similar, not necessarily identical, as in prior studies. Because of the non-identity, two objects may be captured in different environments and domains. Thus, this task also encompasses robust matching under image corruptions and domain shifts. Our method exploits object detection and visual explanation as high-level features, thereby strongly focusing existing feature matchers on objects. Our experiments demonstrated the effectiveness of the proposed method in non-identical object matching and relative pose estimation under various image corruptions.

Acknowledgement. Kazuhiko Kawamoto and Hiroshi Kera were supported by JSPS KAKENHI Grant Numbers JP22H03658 and JP22K17962, respectively. They were also supported by Ricoh Company, Ltd.

References

- [1] Samira Abnar and Willem Zuidema. Quantifying Attention Flow in Transformers. In *Association for Computational Linguistics*, 2020. 8
- [2] Mehmet Aygun and Oisín Mac Aodha. Demystifying Unsupervised Semantic Correspondence Estimation. In *European Conference on Computer Vision (ECCV)*, 2022. 3
- [3] Aditya Chattopadhyay, Anirban Sarkar, Prantik Howlader, and Vineeth N Balasubramanian. Grad-CAM++: Generalized Gradient-Based Visual Explanations for Deep Convolutional Networks. In *Proceedings of the IEEE Winter Conference on Applications of Computer Vision (WACV)*, 2018. 8
- [4] Chen, Hongkai, Luo, Zixin, Zhang, Jiahui, Zhou, Lei, Bai, Xuyang, Hu, Zeyu, Tai, Chiew-Lan, Quan, and Long. Learning to Match Features with Seeded Graph Matching Network. *Proceedings of the IEEE/CVF International Conference on Computer Vision (ICCV)*, 2021. 4, 6, 7
- [5] Hongkai Chen, Zixin Luo, Lei Zhou, Yurun Tian, Mingmin Zhen, Tian Fang, David Mckinnon, Yanghai Tsin, and Long Quan. ASpanFormer: Detector-Free Image Matching with Adaptive Span Transformer. In *European Conference on Computer Vision (ECCV)*, 2022. 1, 3
- [6] Seokju Cho, Sunghwan Hong, Sangryul Jeon, Yunsung Lee, Kwanghoon Sohn, and Seungryong Kim. CATs: Cost Aggregation Transformers for Visual Correspondence. In *Neural Information Processing Systems (NeurIPS)*, 2021. 3
- [7] Seokju Cho, Sunghwan Hong, and Seungryong Kim. CATs++: Boosting Cost Aggregation With Convolutions and Transformers. *IEEE Transactions on Pattern Analysis and Machine Intelligence*, 2023. 1, 3
- [8] Davison, Andrew J., Reid, Ian D., Molton, Nicholas D., Stasse, and Olivier. MonoSLAM: Real-Time Single Camera SLAM. *IEEE Transactions on Pattern Analysis and Machine Intelligence*, 2007. 2
- [9] Jia Deng, Wei Dong, Richard Socher, Li-Jia Li, Kai Li, and Li Fei-Fei. ImageNet: A large-scale hierarchical image database. In *Proceedings of the IEEE/CVF Conference on Computer Vision and Pattern Recognition (CVPR)*, 2009. 6, 1, 2, 3, 4
- [10] Daniel DeTone, Tomasz Malisiewicz, and Andrew Rabinovich. SuperPoint: Self-Supervised Interest Point Detection and Description. In *Proceedings of the IEEE/CVF Conference on Computer Vision and Pattern Recognition (CVPR)*, 2018. 1, 2, 6, 7, 3, 4, 5
- [11] Johan Edstedt, Qiyu Sun, Georg Bökman, Mårten Wadenbäck, and Michael Felsberg. RoMa: Robust Dense Feature Matching. *arXiv preprint arXiv:2305.15404*, 2023. 1, 3
- [12] Johan Edstedt, Georg Bökman, and Zhenjun Zhao. DeDoDe v2: Analyzing and Improving the DeDoDe Keypoint Detector. In *Proceedings of the IEEE/CVF Conference on Computer Vision and Pattern Recognition Workshops (CVPRW)*, 2024. 2
- [13] Martin A Fischler and Robert C Bolles. Random sample consensus: a paradigm for model fitting with applications to image analysis and automated cartography. In *Communications of the ACM*, 1981. 7
- [14] Pierre Gleize, Weiyao Wang, and Matt Feiszli. SiLK – Simple Learned Keypoints. In *Proceedings of the IEEE/CVF International Conference on Computer Vision (ICCV)*, 2023. 2
- [15] Bumsu Ham, Minsu Cho, Cordelia Schmid, and Jean Ponce. Proposal Flow: Semantic Correspondences from Object Proposals. In *arXiv:1703.07144*, 2017. 3
- [16] Kai Han, Rafael S. Rezende, Bumsu Ham, Kwan-Yee K. Wong, Minsu Cho, Cordelia Schmid, and Jean Ponce. SCNet: Learning Semantic Correspondence. In *Proceedings of the IEEE/CVF International Conference on Computer Vision (ICCV)*, 2017. 3
- [17] Yuze He, Yubin Hu, Wang Zhao, Jisheng Li, Yong-Jin Liu, Yuxing Han, and Jiangtao Wen. DarkFeat: Noise-Robust Feature Detector and Descriptor for Extremely Low-Light RAW Images. In *Association for the Advancement of Artificial Intelligence (AAAI)*, 2023. 1, 2, 3
- [18] Hedlin, Eric, Sharma, Gopal, Mahajan, Shweta, He, Xingzhe, Isack, Hossam, Rhodin, Abhishek Kar Helge, Tagliasacchi, Andrea, Yi, and Kwang Moo. Unsupervised Keypoints from Pretrained Diffusion Models. *arXiv preprint arXiv:2312.00065*, 2023. 2
- [19] Eric Hedlin, Gopal Sharma, Shweta Mahajan, Hossam Isack, Abhishek Kar, Andrea Tagliasacchi, and Kwang Moo Yi. Unsupervised Semantic Correspondence Using Stable Diffusion. In *Neural Information Processing Systems (NeurIPS)*, 2023. 3
- [20] Dan Hendrycks and Thomas Dietterich. Benchmarking Neural Network Robustness to Common Corruptions and Perturbations. In *Proceedings of the International Conference on Learning Representations (ICLR)*, 2019. 2, 3, 6, 7, 8, 1, 4
- [21] Sunghwan Hong, Seokju Cho, Seungryong Kim, and Stephen Lin. Unifying Feature and Cost Aggregation with Transformers for Semantic and Visual Cor-

- respondence. In *Proceedings of the International Conference on Learning Representations (ICLR)*, 2024. 3
- [22] Hanwen Jiang, Arjun Karapur, Bingyi Cao, Qixing Huang, and Andre Araujo. OmniGlue: Generalizable Feature Matching with Foundation Model Guidance. In *Proceedings of the IEEE/CVF Conference on Computer Vision and Pattern Recognition (CVPR)*, 2024. 1
- [23] Wei Jiang, Eduard Trulls, Jan Hosang, Andrea Tagliasacchi, and Kwang Moo Yi. COTR: Correspondence Transformer for Matching Across Images. In *Proceedings of the IEEE/CVF International Conference on Computer Vision (ICCV)*, 2021. 1, 3
- [24] Alexander Kirillov, Eric Mintun, Nikhila Ravi, Hanzi Mao, Chloe Rolland, Laura Gustafson, Tete Xiao, Spencer Whitehead, Alexander C. Berg, Wan-Yen Lo, Piotr Dollár, and Ross Girshick. Segment Anything. *arXiv:2304.02643*, 2023. 8
- [25] Zhengqi Li and Noah Snavely. MegaDepth: Learning Single-View Depth Prediction from Internet Photos. In *Proceedings of the IEEE/CVF Conference on Computer Vision and Pattern Recognition (CVPR)*, 2018. 7
- [26] Tsung-Yi Lin, Michael Maire, Serge J. Belongie, Lubomir D. Bourdev, Ross B. Girshick, James Hays, Pietro Perona, Deva Ramanan, Piotr Dollár, and C. Lawrence Zitnick. Microsoft COCO: Common Objects in Context. *CoRR*, 2014. 6, 1, 2, 3, 4
- [27] Philipp Lindenberger, Paul-Edouard Sarlin, and Marc Pollefeys. LightGlue: Local Feature Matching at Light Speed. In *Proceedings of the IEEE/CVF International Conference on Computer Vision (ICCV)*, 2023. 1, 2, 3, 4, 5, 6, 7, 8
- [28] David G Lowe. Distinctive image features from scaleinvariant keypoints. In *International Journal of Computer Vision (IJCV)*, 2004. 2
- [29] Xiaoyong Lu and Songlin Du. Raising the Ceiling: Conflict-Free Local Feature Matching with Dynamic View Switching. In *European Conference on Computer Vision (ECCV)*, 2024. 3
- [30] Xiaoyong Lu, Yaping Yan, Tong Wei, and Songlin Du. Scene-Aware Feature Matching, 2023. 1, 3
- [31] Lundberg, Scott M., Lee, and Su-In. A Unified Approach to Interpreting Model Predictions. In *Neural Information Processing Systems (NeurIPS)*, 2017. 8
- [32] Grace Luo, Lisa Dunlap, Dong Huk Park, Aleksander Holynski, and Trevor Darrell. Diffusion Hyperfeatures: Searching Through Time and Space for Semantic Correspondence. In *Neural Information Processing Systems (NeurIPS)*, 2023. 1, 3
- [33] Juhong Min, Jongmin Lee, Jean Ponce, and Minsu Cho. Hyperpixel Flow: Semantic Correspondence with Multi-layer Neural Features. In *Proceedings of the IEEE/CVF International Conference on Computer Vision (ICCV)*, 2019. 3
- [34] Guillaume Le Moing, Jean Ponce, and Cordelia Schmid. Dense Optical Tracking: Connecting the Dots. *arXiv preprint arXiv:2312.00786*, 2023. 2
- [35] Raúl Mur-Artal, J. M. M. Montiel, and Juan D. Tardós. ORB-SLAM: A Versatile and Accurate Monocular SLAM System. In *IEEE Transactions on Robotics*, 2015. 2
- [36] Junjie Ni, Guofeng Zhang, Guanglin Li, Yijin Li, Xinyang Liu, Zhaoyang Huang, and Hujun Bao. ETO:Efficient Transformer-based Local Feature Matching by Organizing Multiple Homography Hypotheses. In *European Conference on Computer Vision (ECCV)*, 2024. 3
- [37] Maxime Oquab, Timothée Darcet, Theo Moutakanni, Huy V. Vo, Marc Szafraniec, Vasil Khalidov, Pierre Fernandez, Daniel Haziza, Francisco Massa, Alaaeldin El-Nouby, Russell Howes, Po-Yao Huang, Hu Xu, Vasu Sharma, Shang-Wen Li, Wojciech Galuba, Mike Rabbat, Mido Assran, Nicolas Ballas, Gabriel Synnaeve, Ishan Misra, Herve Jegou, Julien Mairal, Patrick Labatut, Armand Joulin, and Piotr Bojanowski. DINOv2: Learning Robust Visual Features without Supervision, 2023. 3
- [38] Rémi Pautrat, Iago Suárez, Yifan Yu, Marc Pollefeys, and Viktor Larsson. GlueStick: Robust Image Matching by Sticking Points and Lines Together. In *Proceedings of the IEEE/CVF International Conference on Computer Vision (ICCV)*, 2023. 1, 2, 3, 4, 6, 7, 8
- [39] William Peebles, Jun-Yan Zhu, Richard Zhang, Antonio Torralba, Alexei Efros, and Eli Shechtman. GAN-Supervised Dense Visual Alignment. In *Proceedings of the IEEE/CVF Conference on Computer Vision and Pattern Recognition (CVPR)*, 2022. 3
- [40] Gabriel Peyré and Marco Cuturi. Computational Optimal Transport. In *Foundations and Trends® in Machine Learning*, 2019. 3
- [41] Guilherme Potje, Felipe Cadar, André Araujo, Renato Martins, and Erickson R. Nascimento. XFeat: Accelerated Features for Lightweight Image Matching. In *Proceedings of the IEEE/CVF Conference on Computer Vision and Pattern Recognition (CVPR)*, 2024. 2
- [42] Alec Radford, Jong Wook Kim, Chris Hallacy, Aditya Ramesh, Gabriel Goh, Sandhini Agarwal, Girish Sastry, Amanda Askell, Pamela Mishkin, Jack Clark, et al. Learning transferable visual models from natural language supervision. In *International conference on machine learning (ICML)*, 2021. 6
- [43] Umer Rafi, Andreas Doering, Bastian Leibe, and Juer-gen Gall. Self-supervised Keypoint Correspondences for Multi-person Pose Estimation and Tracking in

- Videos. In *European Conference on Computer Vision (ECCV)*, 2020. 2
- [44] Nikhila Ravi, Valentin Gabeur, Yuan-Ting Hu, Ronghang Hu, Chaitanya Ryali, Tengyu Ma, Haitham Khedr, Roman Rädle, Chloe Rolland, Laura Gustafson, Eric Mintun, Junting Pan, Kalyan Vasudev Alwala, Nicolas Carion, Chao-Yuan Wu, Ross Girshick, Piotr Dollár, and Christoph Feichtenhofer. SAM 2: Segment Anything in Images and Videos. *arXiv preprint arXiv:2408.00714*, 2024. 8
- [45] I. Rocco, R. Arandjelović, and J. Sivic. Efficient Neighbourhood Consensus Networks via Submanifold Sparse Convolutions. In *European Conference on Computer Vision (ECCV)*, 2020. 1, 3
- [46] Barbara Roessle and Matthias Nießner. End2End Multi-View Feature Matching with Differentiable Pose Optimization. In *Proceedings of the IEEE/CVF International Conference on Computer Vision (ICCV)*, 2023. 1
- [47] Robin Rombach, Andreas Blattmann, Dominik Lorenz, Patrick Esser, and Björn Ommer. High-Resolution Image Synthesis with Latent Diffusion Models, 2021. 3, 6, 1, 4
- [48] Ethan Rublee, Vincent Rabaud, Kurt Konolige, and Gary Bradski. ORB: An efficient alternative to SIFT or SURF. In *Proceedings of the IEEE/CVF International Conference on Computer Vision (ICCV)*, 2011. 2
- [49] Paul-Edouard Sarlin, Daniel DeTone, Tomasz Malisiewicz, and Andrew Rabinovich. SuperGlue: Learning Feature Matching with Graph Neural Networks. In *Proceedings of the IEEE/CVF Conference on Computer Vision and Pattern Recognition (CVPR)*, 2020. 1, 2, 3, 4
- [50] Johannes Lutz Schonberger and Jan-Michael Frahm. Structure-From-Motion Revisited. In *Proceedings of the IEEE/CVF Conference on Computer Vision and Pattern Recognition (CVPR)*, 2016. 2, 7
- [51] Ramprasaath R. Selvaraju, Michael Cogswell, Abhishek Das, Ramakrishna Vedantam, Devi Parikh, and Dhruv Batra. Grad-CAM: Visual Explanations from Deep Networks via Gradient-based Localization. In *Proceedings of the IEEE/CVF International Conference on Computer Vision (ICCV)*, 2017. 2, 4, 6
- [52] Aleksandar Shtedritski, Andrea Vedaldi, and Christian Rupprecht. Learning Universal Semantic Correspondences with No Supervision and Automatic Data Curation. In *Proceedings of the IEEE/CVF International Conference on Computer Vision (ICCV) Workshops*, 2023. 3
- [53] Jianlin Su, Yu Lu, Shengfeng Pan, Ahmed Murtadha, Bo Wen, and Yunfeng Liu. RoFormer: Enhanced Transformer with Rotary Position Embedding. In *arXiv preprint arXiv:2104.09864*, 2021. 5
- [54] Kosuke Sumiyasu, Kazuhiko Kawamoto, and Hiroshi Kera. Identifying Important Group of Pixels using Interactions, 2024. 8
- [55] Sun, Jiaming, Wang, Zihao, Zhang, Siyu, He, Xingyi, Zhao, Hongcheng, Zhang, Guofeng, Zhou, and Xiaowei. OnePose: One-Shot Object Pose Estimation without CAD Models. *Proceedings of the IEEE/CVF Conference on Computer Vision and Pattern Recognition (CVPR)*, 2022. 2
- [56] Jiaming Sun, Zehong Shen, Yuang Wang, Hujun Bao, and Xiaowei Zhou. LoFTR: Detector-Free Local Feature Matching with Transformers. In *Proceedings of the IEEE/CVF Conference on Computer Vision and Pattern Recognition (CVPR)*, 2021. 1, 2, 3, 6, 7, 8
- [57] Jiaming Sun, Zihao Wang, Siyu Zhang, Xingyi He, Hongcheng Zhao, Guofeng Zhang, and Xiaowei Zhou. OnePose: One-Shot Object Pose Estimation without CAD Models. In *Proceedings of the IEEE/CVF Conference on Computer Vision and Pattern Recognition (CVPR)*, 2022. 2
- [58] Luming Tang, Menglin Jia, Qianqian Wang, Cheng Peng Phoo, and Bharath Hariharan. Emergent Correspondence from Image Diffusion. In *Neural Information Processing Systems (NeurIPS)*, 2023. 3
- [59] Michał J. Tyszkiewicz, Pascal Fua, and Eduard Trulls. DISK: Learning local features with policy gradient. In *Neural Information Processing Systems (NeurIPS)*, 2020. 2
- [60] Ashish Vaswani, Noam Shazeer, Niki Parmar, Jakob Uszkoreit, Llion Jones, Aidan N. Gomez, Lukasz Kaiser, and Illia Polosukhin. Attention Is All You Need. In *Neural Information Processing Systems (NeurIPS)*, 2017. 3
- [61] Wang, Xinjiang, Liu, Zeyu, Hu, yu, Xi, Wei, Yu, Wenxian, Zou, and Danping. FeatureBooster: Boosting Feature Descriptors with a Lightweight Neural Network. In *Proceedings of the IEEE/CVF Conference on Computer Vision and Pattern Recognition (CVPR)*, 2023. 2
- [62] Chien-Yao Wang, Alexey Bochkovskiy, and Hong-Yuan Mark Liao. YOLOv7: Trainable bag-of-freebies sets new state-of-the-art for real-time object detectors. In *Proceedings of the IEEE/CVF Conference on Computer Vision and Pattern Recognition (CVPR)*, 2023. 2, 4, 6
- [63] Qianqian Wang, Yen-Yu Chang, Ruojin Cai, Zhengqi Li, Bharath Hariharan, Aleksander Holynski, and Noah Snavely. Tracking Everything Everywhere All at Once. In *Proceedings of the IEEE/CVF International Conference on Computer Vision (ICCV)*, 2023. 2

- [64] Yifan Wang, Xingyi He, Sida Peng, Dongli Tan, and Xiaowei Zhou. Efficient LoFTR: Semi-Dense Local Feature Matching with Sparse-Like Speed. In *Proceedings of the IEEE/CVF Conference on Computer Vision and Pattern Recognition (CVPR)*, 2024. [2](#), [3](#), [6](#), [8](#), [1](#), [7](#)
- [65] Shibiao Xu, Shunpeng Chen, Rongtao Xu, Changwei Wang, Peng Lu, and Li Guo. Local Feature Matching Using Deep Learning: A Survey, 2024. [3](#)
- [66] Fei Xue, Ignas Budvytis, and Roberto Cipolla. IMP: Iterative Matching and Pose Estimation with Adaptive Pooling. In *Proceedings of the IEEE/CVF Conference on Computer Vision and Pattern Recognition (CVPR)*, 2023. [1](#)
- [67] Jiahuan Yu, Jiahao Chang, Jianfeng He, Tianzhu Zhang, and Feng Wu. Adaptive Spot-Guided Transformer for Consistent Local Feature Matching. In *Proceedings of the IEEE/CVF Conference on Computer Vision and Pattern Recognition (CVPR)*, 2023. [1](#), [3](#)
- [68] Liao Yun, Di Yide, Zhu Kaijun, Zhou Hao, Lu Mingyu, Zhang Yijia, Qing Duan, and Liu Junhui. Local feature matching from detector-based to detector-free: a survey. *Applied Intelligence*, 2024. [3](#)
- [69] Junyi Zhang, Charles Herrmann, Junhwa Hur, Luisa Polania Cabrera, Varun Jampani, Deqing Sun, and Ming-Hsuan Yang. A Tale of Two Features: Stable Diffusion Complements DINO for Zero-Shot Semantic Correspondence. In *Neural Information Processing Systems (NeurIPS)*, 2023. [3](#)
- [70] Junyi Zhang, Charles Herrmann, Junhwa Hur, Eric Chen, Varun Jampani, Deqing Sun, and Ming-Hsuan Yang. Telling Left from Right: Identifying Geometry-Aware Semantic Correspondence. In *Proceedings of the IEEE/CVF Conference on Computer Vision and Pattern Recognition (CVPR)*, 2024. [1](#), [2](#), [3](#)
- [71] Yesheng Zhang and Xu Zhao. MESA: Matching Everything by Segmenting Anything. In *Proceedings of the IEEE/CVF Conference on Computer Vision and Pattern Recognition (CVPR)*, 2024. [3](#)
- [72] Yesheng Zhang, Xu Zhao, and Dahong Qian. Searching from Area to Point: A Hierarchical Framework for Semantic-Geometric Combined Feature Matching. In *arXiv preprint arXiv:2305.00194*, 2023. [1](#), [3](#)
- [73] Zhou, Bolei, Khosla, Aditya, Lapedriza, Agata, Oliva, Aude, Torralba, and Antonio. Learning deep features for discriminative localization. In *Proceedings of the IEEE Conference on Computer Vision and Pattern Recognition (CVPR)*, 2016. [8](#)
- [74] Qunjie Zhou, Torsten Sattler, and Laura Leal-Taixe. Patch2Pix: Epipolar-Guided Pixel-Level Correspondences. In *Proceedings of the IEEE/CVF Conference on Computer Vision and Pattern Recognition (CVPR)*, 2021. [1](#), [3](#)

Matching Non-Identical Objects

Supplementary Material

A. Additional matching results

In Sec. 5.1 of the main text, we evaluated non-identical object matching by inserting our method between SuperPoint [10] and LightGlue [27]. Here, “Ours” in the results refers to the case where only our weighting module is used, without applying the class similarity adapter. The matching results for various image pair show that our method enhances matchers and provides dense and consistent correspondences. To demonstrate this generality for various image pairs, we show more results in three cases: (i) same class (i.e., $y_A = y_B, D_A = D_B$), (ii) class discrepancy (i.e., $y_A \neq y_B, D_A = D_B$), (iii) domain shift (i.e., $o_A \equiv o_B, D_A \neq D_B$). Additionally, we present more results for complex scenes containing multiple objects in a single image.

Setup. We collected various images with objects from the COCO [26] and ImageNet [9] datasets. To prepare drawing or sketch versions of several images, we used the DreamStudio³, which is backed by the Stable Diffusion [47]. For details of the experiment, refer to Sec. 5.1.

A.1. Success cases

Figure A shows the matching results for the same class case. As in the main text, The introduction of the proposed method turns sparse and inconsistent matching into dense and consistent one. The combination of SuperPoint and LightGlue with our method is robust to object color and shape differences and performs dense and consistent matching. Even in the case with class discrepancy, as shown in Fig. B, the proposed method successfully corresponds the same parts (e.g., eyes to eyes, nose to nose) between various animals. Figure C shows the case of domain shift between images, where our method reduces mismatching caused by image corruptions and image style changes (e.g., photos and drawings). Figure D shows cases where multiple objects are present in an image, demonstrating that our class similarity adapter selects semantically similar object pairs and provides condensed matching between the two objects. These results indicate that the proposed method can perform accurate matching in many cases under the challenging condition of non-identical object matching.

A.2. Failure cases

There are some cases of failure in non-identical object matching, as shown in Fig. E. It is difficult to match objects that are of the same class but have significantly different shapes (e.g., the presence or absence of an airplane

propeller) or objects that are similar in color or size to other parts (e.g., eyes and nose that are small, round, and black) of the object. Furthermore, image corruptions sometimes hide the texture of the objects, making it difficult to pinpoint the areas to be matched.

B. Robust image matching details

With the same setup in Sec. 5.2 of the main text, we evaluate the effectiveness of the proposed method for LightGlue [27] and GlueStick [38] on the robustness to image corruptions and domain shift in image matching. Here, we consider the maximum angular error at 10° and 5° instead of 20°. The results of relative pose estimation with common corruptions [20] on one or both of the input images in the MegaDepth-1500 [56] show that the proposed method improves the robustness of LightGlue and GlueStick. In all experiments, we used the pretrained sparse matchers LightGlue [27], and GlueStick [38], and the dense matchers LoFTR [56] and EfficientLoFTR [64], downloaded from their official repositories.⁴

B.1. Robustness against common corruptions

In this experiment, common corruptions are added to both input images to demonstrate robustness against corruption. Table A shows the results of relative pose estimation for maximum angular error of 10° and 5°. As the results show, the proposed method makes the LightGlue and GlueStick robust against most types of common corruptions (roughly, 5% to 10% increase) with a slight decrease in clean accuracy. For the Noise category, LightGlue and GlueStick with our method even surpass dense matchers in both cases.

B.2. Robustness against environmental changes

In contrast to Appendix B.1, in this experiment, common corruptions are added to one of the image pairs to demonstrate robustness against domain shift between images. Table B shows the results of relative pose estimation for maximum angular error of 10° and 5°. As the results show, the proposed method is robust to LightGlue and GlueStick, and in particular, significantly improves the AUC of the former for all Noise, Blur, and Digital categories, and the latter for all Noise and Blur categories. For the Noise category, LightGlue and GlueStick with our method even exceeds dense matchers in both cases.

⁴LightGlue: <https://github.com/cvg/LightGlue>
GlueStick: <https://github.com/cvg/GlueStick>
LoFTR: <https://github.com/zju3dv/LoFTR>
ELoFTR: <https://github.com/zju3dv/efficientloftr>

³DreamStudio: <https://beta.dreamstudio.ai/generate>

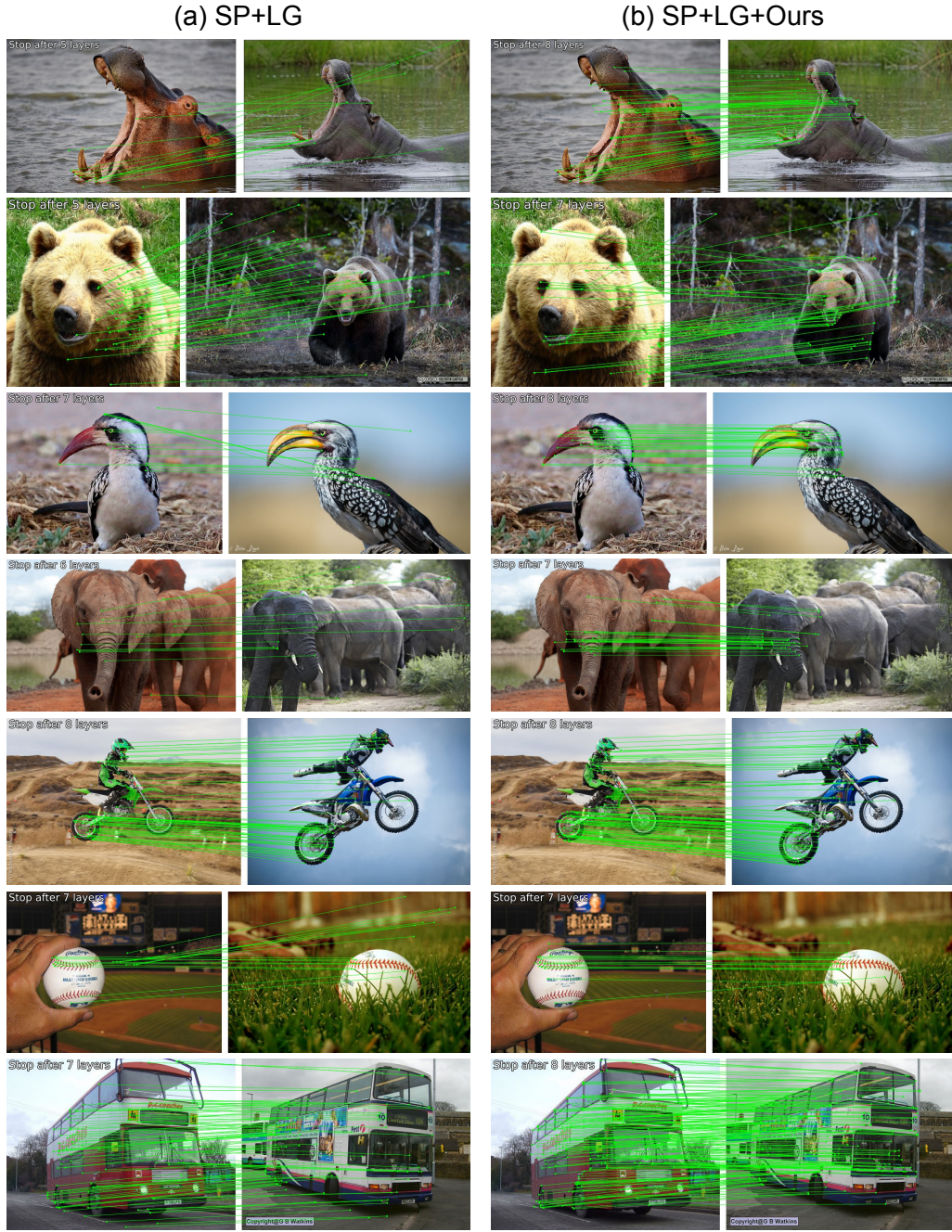


Figure A. Matching results in the same class case. Image pairs show objects of the same class in ImageNet [9] or COCO [26] datasets. (a) A combination of SuperPoint (SP) [10] and LightGlue (LG) [27] only finds a small number of correspondence, and many of them are incorrect. (b) The proposed method significantly improves the matching and performs dense and consistent correspondences.

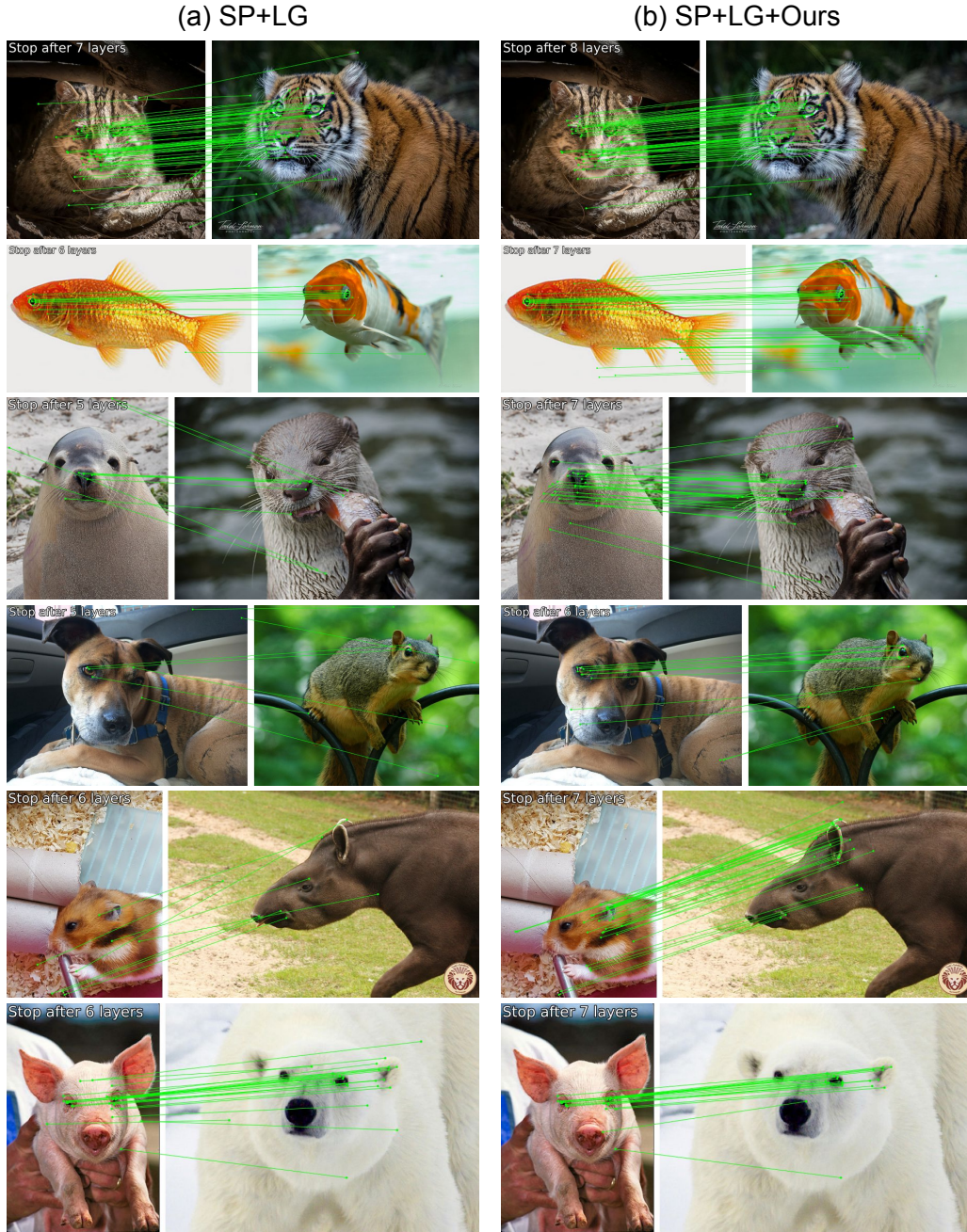


Figure B. Matching results in the class discrepancy case. Image pairs show objects with class discrepancies in ImageNet [9] or COCO [26] datasets. (a) A combination of SuperPoint (SP) [10] and LightGlue (LG) [27] finds many inconsistent and scattered matches, and it is unclear which is the correct correspondence. (b) The proposed method finds almost all matches for the corresponding parts of the animal, which largely improves the matching to consistency.



Figure C. Matching results in the domain shift case. Image pairs for matching are ImageNet [9] or COCO [26] datasets with common corruptions [20], and illustrations or sketches of a motorcycle, a violin, and a cat are generated by the Stable Diffusion [47]. (a) A combination of SuperPoint (SP) [10] and LightGlue (LG) [27] finds correct matching, but also finds mismatches with many non-correspondence areas. (b) The proposed method reduces these mismatches and further improves to denser matching between objects.

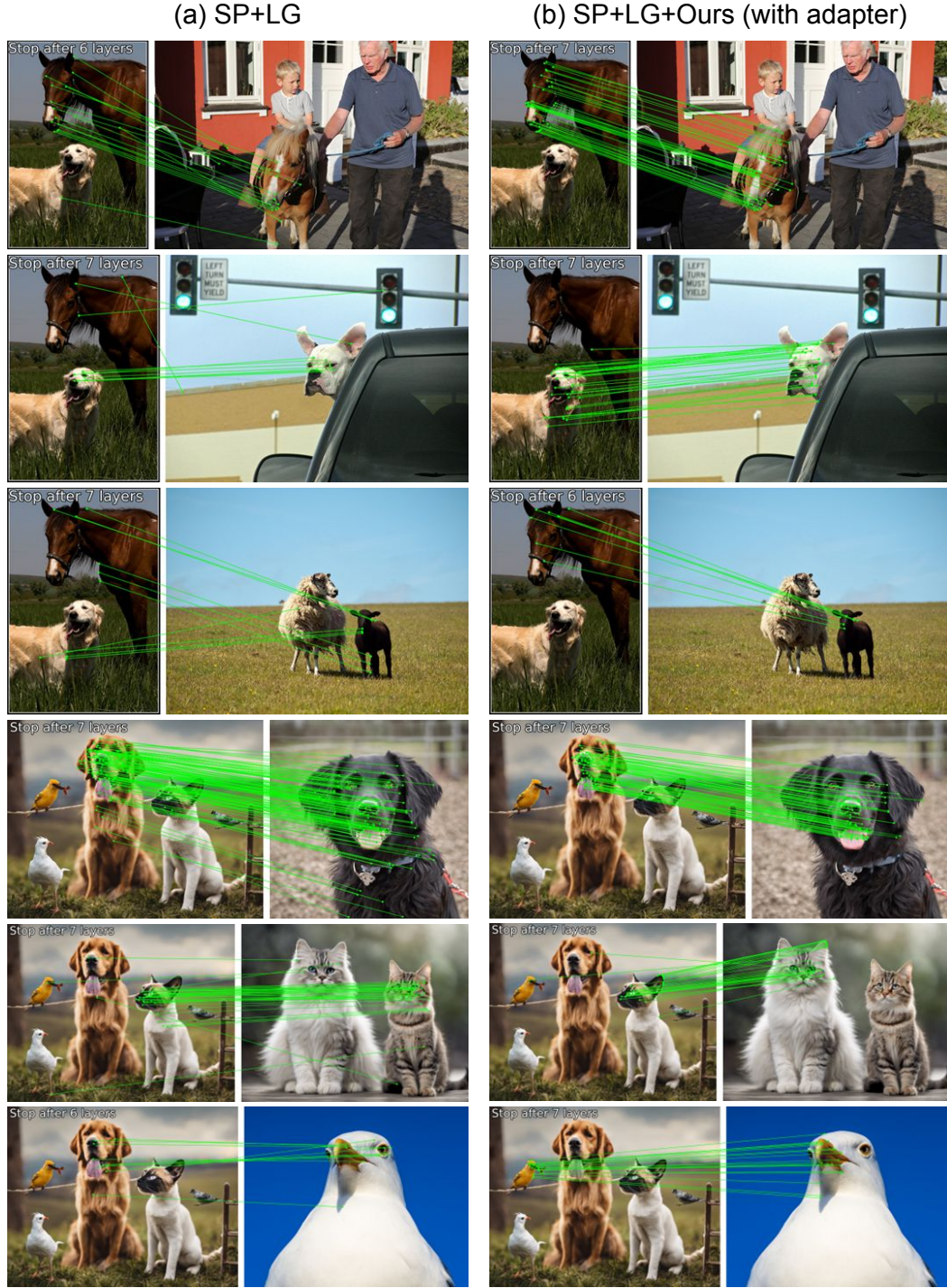


Figure D. Matching results in complex scenes containing multiple objects. (a) A combination of SuperPoint (SP) [10] and LightGlue (LG) [27] causes correspondences to scatter across multiple objects. (b) The proposed class similarity adapter effectively selects semantically similar object pairs and provides condensed and consistent matching between the relevant parts of the objects.



Figure E. Failure cases of non-identical object matching. (a) A combination of SuperPoint (SP) [10] and LightGlue (LG) [27] fails in matching. (b) The proposed method improves several matching but still leaves many corresponding areas unmatched.

Table A. The pose accuracy (AUC) at the maximum angular error of 10° and 5° of the relative pose estimation from image pairs MegaDepth-1500 [56] under common corruptions. Both images are corrupted with the same type of corruption. Our method largely improves LightGlue (LG) [27] and GlueStick (GS) [38] for most categories and the average AUC. The results of a dense matchers, LoFTR [56] and Efficient LoFTR (ELoFTR) [64], are shown for reference. Our method improves the robustness of sparse matchers with a marginal decrease in clean accuracy.

Common Corruptions	AUC@ 10° with pairs of corrupted images					
	<i>keypoint detector : SuperPoint</i>				<i>dense matcher</i>	
	LG	LG+Ours	GS	GS+Ours	LoFTR	ELoFTR
None (Clean)	67.89	66.98	64.11	61.94	68.88	72.18
Gaussian Noise	27.44	37.28	28.64	35.11	20.07	20.32
Shot Noise	27.07	39.79	27.81	33.42	24.27	23.89
Impulse Noise	28.70	37.25	29.10	34.44	22.27	23.75
Defocus Blur	18.58	24.51	30.12	33.78	43.27	40.33
Frosted Glass Blur	17.24	27.61	29.16	31.75	39.21	30.43
Motion Blur	27.08	34.85	27.98	35.46	40.68	38.01
Zoom Blur	12.50	20.23	12.64	20.72	12.01	13.66
Snow	18.35	12.56	12.46	10.49	18.94	24.27
Frost	20.86	18.75	17.64	15.48	11.15	15.67
Fog	56.32	62.62	55.14	57.24	53.05	59.85
Brightness	61.10	63.95	58.75	56.51	61.88	67.22
Contrast	24.33	23.10	24.31	27.45	38.57	44.78
Elastic Transform	36.76	47.02	41.53	45.52	41.27	42.79
Pixelate	51.60	60.66	47.60	47.32	62.55	64.85
JPEG Compression	16.60	27.73	22.35	27.64	43.49	43.50
Average	29.64	35.86	31.02	34.16	35.51	36.89

AUC@ 5° with pairs of corrupted images						
None (Clean)	50.43	49.71	45.92	43.11	52.52	56.38
Gaussian Noise	14.70	24.44	14.63	21.53	9.85	9.57
Shot Noise	13.71	23.44	13.44	18.06	12.21	11.78
Impulse Noise	15.65	21.25	16.90	20.64	10.92	11.77
Defocus Blur	8.22	11.69	16.59	20.64	27.77	25.67
Frosted Glass Blur	7.17	18.09	14.58	16.12	24.59	16.17
Motion Blur	14.72	20.72	15.26	22.34	25.37	27.82
Zoom Blur	5.38	8.82	6.02	14.16	5.17	8.42
Snow	9.48	8.32	5.92	3.87	9.91	13.79
Frost	11.92	11.29	9.92	7.72	6.09	8.75
Fog	39.01	43.43	35.88	37.58	36.94	48.00
Brightness	43.60	47.98	41.86	39.60	45.13	50.73
Contrast	11.69	13.93	12.75	15.29	23.13	29.26
Elastic Transform	20.43	29.64	24.29	27.28	24.40	25.35
Pixelate	32.97	41.82	29.86	29.66	46.40	48.41
JPEG Compression	8.00	15.94	9.71	14.79	27.77	27.45
Average	17.11	22.72	17.84	20.62	22.38	24.20

Table B. The pose accuracy (AUC) at the maximum angular error of 10° and 5° of the relative pose estimation from image pairs MegaDepth-1500 [56] under common corruptions. Only one of the input images is corrupted and the other is a clean image. Our method largely improves LightGlue (LG) [27] and GlueStick (GS) [38] for most categories and the average AUC. The results of dense matchers, LoFTR [56], and Efficient LoFTR (ELoFTR) [64] are shown for reference. Our method improves the robustness of sparse matchers with a marginal decrease in clean accuracy.

Common Corruptions	AUC@ 10° with pairs of clean and corrupted images					
	<i>keypoint detector : SuperPoint</i>				<i>dense matcher</i>	
	LG	LG+Ours	GS	GS+Ours	LoFTR	ELoFTR
None (Clean)	67.89	66.98	64.11	61.94	68.88	72.18
Gaussian Noise	16.63	28.34	28.57	32.42	24.17	27.01
Shot Noise	19.97	32.50	26.23	29.92	26.58	29.11
Impulse Noise	23.56	34.74	33.12	36.26	25.67	28.67
Defocus Blur	8.29	22.43	12.03	18.17	36.85	31.36
Frosted Glass Blur	19.00	32.78	26.39	29.66	40.40	34.59
Motion Blur	33.29	39.69	27.88	38.30	39.41	37.15
Zoom Blur	20.38	26.23	16.76	25.67	21.60	21.63
Snow	39.74	41.07	30.74	33.00	35.91	43.33
Frost	47.61	51.78	38.80	41.62	32.97	38.00
Fog	62.39	64.08	61.11	60.80	60.74	65.26
Brightness	63.40	61.75	62.69	60.04	65.64	69.24
Contrast	27.81	33.12	25.86	28.95	30.27	40.35
Elastic Transform	47.62	56.66	52.17	55.08	53.61	56.20
Pixelate	50.14	56.68	50.33	48.63	63.14	66.22
JPEG Compression	29.92	40.31	40.93	40.61	53.58	57.23
Average	33.98	41.48	35.57	38.61	40.70	43.02

Common Corruptions	AUC@ 5° with pairs of clean and corrupted images					
	<i>keypoint detector : SuperPoint</i>				<i>dense matcher</i>	
	LG	LG+Ours	GS	GS+Ours	LoFTR	ELoFTR
None (Clean)	50.43	49.71	45.92	43.11	52.52	56.38
Gaussian Noise	8.42	20.10	16.51	20.52	16.68	18.54
Shot Noise	10.30	20.52	16.14	19.31	18.14	19.72
Impulse Noise	12.88	24.11	21.41	25.35	17.75	19.55
Defocus Blur	3.22	17.92	5.95	15.89	24.73	21.55
Frosted Glass Blur	8.56	22.42	15.54	18.79	26.87	22.61
Motion Blur	18.95	26.22	13.94	24.36	25.92	28.77
Zoom Blur	9.81	19.27	8.95	17.68	15.03	17.16
Snow	22.94	26.90	17.27	20.56	23.94	31.62
Frost	31.58	37.80	24.13	27.95	23.07	29.96
Fog	44.49	45.00	42.65	41.24	44.04	51.15
Brightness	46.14	45.24	43.91	41.63	48.85	52.85
Contrast	14.98	17.15	14.46	17.53	21.09	27.79
Elastic Transform	29.34	39.29	32.27	35.11	36.41	38.80
Pixelate	31.51	38.02	31.82	30.10	46.26	49.92
JPEG Compression	15.86	27.55	22.24	21.87	37.35	40.35
Average	20.60	28.50	21.81	25.19	28.41	31.36